04.2

A model for calculating neutral helium radiation for the Globus-M2 tokamak peripheral plasma spectroscopic diagnostics

© V.M. Timokhin, D.D. Korobko, E.A. Anufriev, V.Yu. Sergeev

Peter the Great Saint-Petersburg Polytechnic University, St. Petersburg, Russia
E-mail: V.Timokhin@spbstu.ru

Received April 4, 2024
Revised May 20, 2024
Accepted May 20, 2024

A simple model has been developed for calculating synthetic images of neutral helium clouds recorded by spectroscopic diagnostics of peripheral distributions of electron temperature and concentration at the Globus-M2 tokamak. The size of the numerically obtained radiating helium cloud is in a quite good agreement with experimental results. Calculations of the effect of averaging the radiation intensity along the line of sight on the recovered electron temperature values demonstrate the need to reduce the angular broadening of the injected helium jet to 10−15°; in this case, the relative measurement error will not exceed 10−20%. As a means for practical engineering implementation of such a helium jet, a Laval nozzle with a set of diaphragms is proposed.

Keywords: helium spectroscopy, radiation modeling, coronal model, gas puff.

DOI: 10.61011/TPL.2024.09.59152.19943

Spectroscopic diagnostics of peripheral plasma with injecting neutral helium provides information on the electron temperature and concentration distributions in the plasma column peripheral regions based on ratios of intensities of the neutral helium emission spectral lines [1]. The provided data on plasma parameters are being averaged along the lines of sight; the size of the light-emitting region along these lines of sight depends on the neutral helium distribution, optical system focal depth, and parameters of plasma in the emitting region. A similar diagnostics have been successfully applied at a number of facilities for determining electron concentration and temperature at the plasma periphery (RFX-mod [2], ASDEX-Upgrade [3]), as well as in experiments with observing filaments of edge instability modes jcite4.

To estimate the error in averaging the measured concentration and temperature, the problem of modeling polychromator images was solved for preset electron temperature and plasma density distributions, which made it possible to significantly improve interpretation of the diagnostic measurements. The goal of this work was to describe this model and analyze the main results of image simulation via it.

Intensities of the neutral helium lines for singlet and triplet transitions (668 nm ($1s3d(^1\mathrm{D})-1s2p(^1\mathrm{P}^0)$), 728 nm ($1s3s(^1\mathrm{S})-1s2p(^1\mathrm{P}^0)$) and 706 nm ($1s3s(^3\mathrm{S})-1s2p(^3\mathrm{P}^0)$)) differently depend on both the electron temperature and concentration; this allows determining the background plasma parameters from the experimentally measured line intensity ratios (in our case $I_{668\,\mathrm{nm}}/I_{728\,\mathrm{nm}}$, $I_{728\,\mathrm{nm}}/I_{706\,\mathrm{nm}}$) by using calculations via the collision-radiative model (CRM) [3]. Different CRM modifications are able to take into account different numbers of simulated helium atom energy levels and either include in calculation the dynamics of their population or consider only stationary populations. The first experimental results obtained by the neutral helium spectroscopic diagnostics at the Globus-M2 tokamak were described in [1]. To determine spatial distributions of the peripheral-plasma electron concentration and temperature, the result of calculations via stationary CRM from [5] was used, which enabled obtaining reasonable distributions of the measured quantities.

The experiment layout is presented in Fig. 1. Emission from the helium jet introduced by the injection system through a capillary 0.5 mm in diameter vertically along the tokamak Zaxis from the point with coordinates $R = 0.24$ m and $Z = -0.51$ m (the point of reference is in the center of the facility) gets on the camera matrix of a four-channel filter-lens imaging polychromator from the viewing field through the focus of the lens located at coordinates $R = 1.10$ m and $Z = 0.26$ m in the tokamak poloidal cross-section shifted from the helium injection crosssection by toroidal angle $\Delta\varphi = 47.4°$. The neutral helium cloud emits predominantly in the PFR (Private Flux Region) region near the lower X point. Emission is received from the region of the facility equatorial plane at the angle of 40° to it. The distance between the objective lens and injection system capillary is 1.2 m. The experimental design is described in more detail in [1].

To calculate the image of the helium emitting cloud measured in the experiment by the optical system camera, 40×40 lines of sight were laid from the polychromator lens focal plane, in which helium radiation integrated along the line of sight was calculated:

$$I \propto \int \varepsilon(l)dl. \qquad (1)$$

Here I is the radiation integrated along the line of sight, ε is the local helium emissivity, l is the integration variable

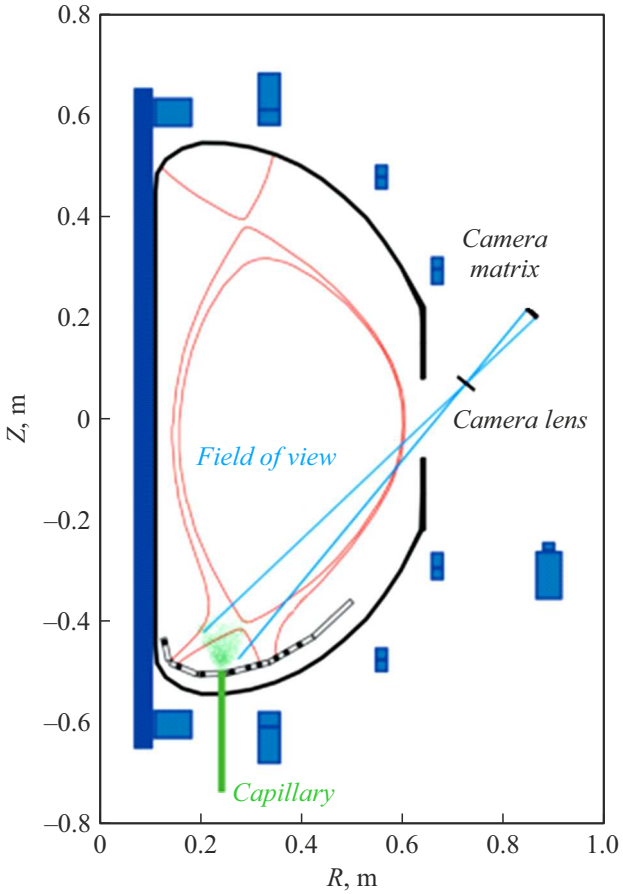

Figure 1. Arrangement of diagnostic elements for the tokamak Globus-M2 peripheral plasma with the neutral helium injection.

(distance along the line of sight). The geometric factor accounting for variations in the angular size of the radiation source that generates the signal in the camera detector was estimated in [6]. It was shown that, because of a large distance between the radiation source and lens (compared to the lens focal length), the geometric factor may be ignored.

Helium radiation is governed by the energy level populations to be calculated, in the general case, according to the complete CRM involving all the essential elementary processes, which is a rather difficult task. In this study, helium radiation was calculated according to a simple coronal model:

$$\varepsilon \sim n \sim n_{\mathrm{He}} n_e \langle \sigma v \rangle. \qquad (2)$$

Here n is the helium level population, n_{He} is the neutral helium concentration, n_e is the electron concentration, $\langle \sigma v \rangle$ is the effective rate coefficient of the helium atom excitation from the ground state to the upper level of the relevant emission line.

Distributions of the electron concentration and temperature in the jet light-emission region were obtained for this calculation by modeling with the SOLPS-ITER code [7] for a discharge similar in parameters to discharge #40269 of the Globus-M2 tokamak where the helium cloud emissions were measured experimentally.

The injectedjet neutral helium concentration distribution versus the opening angle and distance from the capillary was calculated in the approximation of free gas expansion in the collision-free mode under the assumption of a stationary spherical source given in monograph [8]:

$$n_{\mathrm{He}}(\theta, r) = n_0 \cos^2\left(\frac{\pi\theta}{c}\right)\left(\frac{r_0}{r}\right)^2\left(1 - \frac{1}{2S_0}\right). \qquad (3)$$

Angular dependence relative to the injection axis was taken from the same literature source for the case of gas flow in vacuum through a circular hole; it was confirmed by independent calculations for the same conditions and by experimental results (Fig. 2). In formula (3), θ is the angle between the injection axis and radiusvector from the capillary, r is the distance from the capillary outlet, n_0 is the helium concentration at the capillary outlet, r_0 is the capillary radius (0.5 mm), $S_0 = m_{\mathrm{He}} u_0^2 / 2\pi k T_0$, u_0, T_0 are the gas velocity and temperature at the capillary outlet, $c = 2.73$ is the coefficient determining the effective helium-jet full opening angle $2\theta_{\mathrm{He}} = c$ introduced in [8]. The expansion speed is $v_{\mathrm{He}} \approx 1 \cdot 10^3$ m/s which is equal to the sound speed in helium under normal conditions.

To assess the interaction between the jet and tokamak high-temperature plasma, the processes of charge exchange σ_{cx} [9] and ionization through the electron $\langle \sigma_e v_e \rangle$ [10] and ion σ_i [11] channels were taken into account. According to [12], the equation was solved (see below), which accounts for the abovelisted elementary processes in the distribution of neutral helium flowing at constant speed v_{He} from the capillary along its motion trajectory (axis x) according to (3). The model assumes that the neutral helium trajectories are straight-line and start at the point corresponding to the capillary end. The helium outflow space is divided into $N = 50 \times 50 = 2500$ elements of solid angle Ω_i, and each element is related to a single straight-line trajectory. Along these trajectories, the following equation is solved for flow function $F_i(x) = n(x) S_i(x) = n(x) x^2 \Omega_i$:

$$\frac{dF_i(x)}{dx} = -n_e(x)\left(\sigma_i + \sigma_{ex} + \frac{\langle \sigma_e v_e \rangle}{v_{\mathrm{He}}}\right) F_i(x) + \frac{d[n_{\mathrm{He}}(x) x^2 \Omega_i]}{dx}. \qquad (4)$$

Fig. 2, *a* presents an experimentally obtained image of the #40269 discharge jet in the 706 nm spectral line corresponding to transition $1s3s(^3S) - 1s2p(^3P^0)$; the image may be compared with the result of simulation via the abovedescribed model, which is presented in Fig. 2, *b*. Dimensions of the calculated helium emitting cloud are in good agreement with the experimental results; however, there are some discrepancies in the transverse (along R) distribution of the jet glow and in the position of the emission intensity maximum.

Using the concentration and temperature distributions from the SOLPS-ITER code, which more accurately determine the discharge #40269 magnetic configuration, and

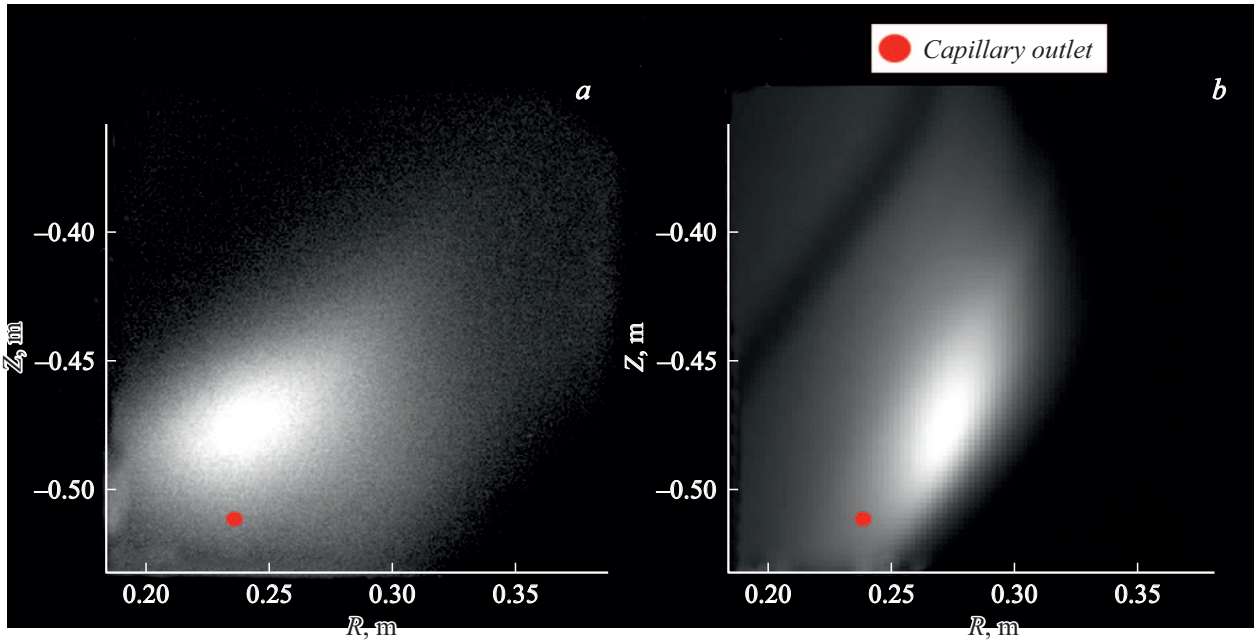

Figure 2. Comparison of experimentally measured helium radiation (a) with that obtained by modeling (b) in discharge #40269 (171 ms).

dynamic CRM which will be soon developed, it is possible to significantly improve the agreement with experimental data under the Globus-M2 tokamak conditions. Nevertheless, the agreement between the calculations of the helium cloud emission intensity distribution and experimental data may be regarded as satisfactory.

In addition, the effect of averaging the emission intensity along the line of sight on the measurements was assessed. Cross sections for transitions from the ground state in which, according to the calculation conditions, the injected jet is located, to the upper transition levels (728 and 706 nm) were taken from the ADAS database [13]. After that, signal ratio $I_{728\,\mathrm{nm}}/I_{706\,\mathrm{nm}}$ was calculated. Electron temperature T_e may be restored from the obtained ratio distribution using the known dependence of ratios $\langle\sigma v_{728\,\mathrm{nm}}\rangle/\langle\sigma v_{706\,\mathrm{nm}}\rangle$ for effective excitation cross sections on T_e.

As per (3), full opening angle $2\theta_{\mathrm{He}}$ of the helium jet is 130°. Calculations were performed at four different opening angles: 12, 18, 24, 130°. In calculations based on the simulated images, plasma parameter profiles were reconstructed with SOLPS-ITER included in the model for calculating the distribution of the neutral helium radiation. Fig. 3 presents the electron temperature along the helium injection axis $T_{e\mathrm{SOLPS}}$ calculated using the SOLPS-ITER code, and electron temperature T_e restored from the simulated images. No data on the excitation cross section are available for temperatures below 5 eV. The figure shows that, in case $2\theta_{\mathrm{He}} = 130°$, the temperature profile reconstructed based on calculations within the framework of the model used in this work appears to be significantly distorted. Relative error of temperature restoration was less than 5% at opening angle $2\theta_{\mathrm{He}} = 12°$, about 20% at $2\theta_{\mathrm{He}} = 18°$, and more than 50% at $2\theta_{\mathrm{He}} = 24°$. Note that the experimentally

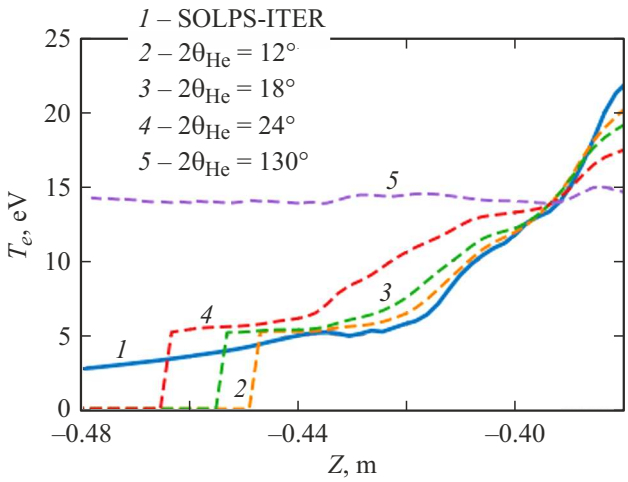

Figure 3. Comparison of the calculated $T_{e\mathrm{SOLPS}}$ and reconstructed T_e temperature profiles along the injection axis for different helium-jet full opening angles $2\theta_{\mathrm{He}}$.

measured jet opening angle (Fig. 2, a) is about 90°, which also prevents reliable reconstruction of the plasma parameter profiles.

The results obtained demonstrate the necessity to reduce the injected helium jet opening angle to 10–15°. For engineering implementation of such a jet geometry, a source designed based on a Laval nozzle with high Mach numbers at the nozzle exit may be considered. In this case, the opening angle will be determined by ratio $2\theta_{\mathrm{He}} \sim \frac{2}{\sqrt{\gamma(\gamma-1)\mathrm{M}^2}}$ [14], where γ is the adiabatic index (5/3 for a monatomic gas), and will meet the requirement for low averaging errors (10–15°). It is also possible to

restrict the helium jet opening angle by using a set of diaphragms as in the helium source for similar diagnostics at the TEXTOR tokamak [15].

Thus, a simple model has been developed for calculating synthetic images of neutral helium cloud emission recorded by spectroscopic diagnostics of the tokamak Globus-M2 peripheral distributions of electron temperature and concentration. Geometric dimensions of the emitting helium cloud obtained as a result of image modeling are in good agreement with experimental results; however, the calculated jet penetration depth is 2−3 cm greater than the experimental values. The necessity of reducing the injected jet opening angle to 10−15°, so as to make the relative measurement error not exceeding 10−20%, has been demonstrated. The available design of the gas puff system can give, jointly with the current diagnostic geometry, the measurement-area temperature values overestimated by 2−3 times. It is proposed to use for engineering implementation of such a helium jet source a Laval nozzle with a set of diaphragms.

Funding

The study was supported by the RF Ministry of Science and Higher Education in the framework of State Assignment in Science (project № FSEG-2024-0005); the study was performed using the Ioffe Institute Federal Common Use Center „Materials Science and Diagnostics in Advanced Technologies“which includes a Unique Scientific Facility „Spherical tokamak Globus-M“.

Conflict of interests

The authors declare that they have no conflict of interests.

References

[1] V.M. Timokhin, V.Yu. Sergeev, E.A. Anufriev, D.D. Korobko, I.A. Sharov, V.I. Varfolomeev, A.N. Novokhatsky, N.N. Bakharev, E.O. Vekshina, K.V. Dolgova, N.S. Zhil'tsov, A.A. Kavin, V.G. Kapralov, E.O. Kiselev, A.N. Koval', G.S. Kurskiev, K.M. Lobanov, V.B. Minaev, I.V. Miroshnikov, E.E. Mukhin, Yu.V. Petrov, V.A. Rozhansky, N.V. Sakharov, V.G. Skokov, A.Yu. Tel'nova, E.E. Tkachenko, V.A. Tokarev, S.Yu. Tolstyakov, E.A. Tyukhmeneva, N.A. Khromov, JETP Lett., **116**, 300 (2022). DOI: 10.1134/S0021364022601592.

[2] M. Agostini, P. Scarin, R. Cavazzana, L. Carraro, L. Grando, C. Taliercio, L. Franchin, A. Tiso, Rev. Sci. Instrum., **86**, 123513 (2015). DOI: 10.1063/1.4939003.

[3] M. Griener, J.M. Muñoz Burgos, M. Cavedon, G. Birkenmeier, R. Dux, B. Kurzan, O. Schmitz, B. Sieglin, U. Stroth, E. Viezzer, E .Wolfrum and the ASDEX Upgrade Team, Plasma Phys. Control. Fusion, **60**, 025008 (2018). DOI: 10.1088/1361-6587/aa97e8.

[4] M. Griener, E. Wolfrum, G. Birkenmeier, M. Faitsch, R. Fischer, G. Fuchert, L. Gil, G.F. Harrer, P. Manz, D. Wendler, U. Stroth, Nucl. Mater. Energy, **25**, 100854 (2020). DOI: 10.1016/j.nme.2020.100854.

[5] W. Zholobenko, M. Rack, D. Reiter, M. Goto, Y. Feng, B. Küppers, P. Börner, Nucl. Fusion, **58**, 126006 (2018). DOI: 10.1088/1741-4326/aadda9.

[6] V.M. Timokhin, E.A. Anufriev, D.D. Korobko, V.Yu. Sergeev, I.A. Sharov, v sb. *Tez. dokl. XX Vseros. konf. „Diagnostika vysokotemperaturnoy plazmy“* (Sochi, 2023), s. 188. (in Russian)

[7] V.A. Rozhansky, S.P. Voskoboynikov, E.G. Kaveeva, D.P. Coster, R. Schneider, Nucl. Fusion, **41**, 387 (2001). DOI: 10.1088/0029-5515/41/4/305.

[8] V.G. Dulov, G.A. Lukýanov, *Gazodinamika processov istecheniya* (Nauka, Novosibirsk, 1984), s. 81, formula (4.18). (in Russian)

[9] K.L. Bell, H.B. Gilbody, J.G. Hughes, A.E. Kingston, F.J. Smith, Phys. Chem. Ref. Data, **12**, 891 (1983). DOI: 10.1063/1.555700.

[10] F.J. Deheer, R. Hoekstra, A.E. Kingston, H.P. Summers, Nucl. Fusion (Suppl.), **3**, 19 (1992).

[11] D. Kaganovich, E. Startsev, R.C. Davidson, New J. Phys., **8**, 278 (2006). DOI: 10.1088/1367-2630/8/11/278.

[12] J. Wesson, *Tokamaks*, 4th ed. (Oxford University Press, 2011).

[13] *Resolved Specific Ion Data Collections in OPEN-ADAS Atomic Data and Analysis Structure* [Electronic resource]. https://open.adas.ac.uk/detail/adf04/helike/helike_idp04he0_t1.dat (access date 22.12.2023).

[14] N.N. Shelukhin, Uch. zap. TsAGI, **10** (2), 130 (1979). (in Russian)

[15] U. Kruezi, H. Stoschus, B. Schweer, G. Sergienko, U. Samm, Rev. Sci. Instrum., **83**, 065107 (2012). DOI: 10.1063/1.4707150.

Translated by EgoTranslating